Journal of Sol-Gel Science and Technology (2024) 111:106–118
https://doi.org/10.1007/s10971-024-06421-w

ORIGINAL PAPER

Termite wings derived N-doped carbon nanodots: applications for Cu2^{+} sensing, fluorescent ink and flexible polymeric film

Jothi Vinoth Kumar[1] · Duraisamy Karthika[2] · V. Arul[3] · K. Radhakrishnan[4] · Pitcheri Rosaiah[5] · Samar A. Aldossari[6] · I. Neelakanta Reddy[7] · Cheolho Bai[7]

Received: 17 April 2024 / Accepted: 10 May 2024 / Published online: 7 June 2024

Abstract

This study used a simple hydrothermal approach to create nitrogen-doped carbon nanodots (TWNCNDs) from termite wings. The TWNCNDs have high fluorescence (FL) quality with a quantum yield of 11.8%. In order to detect Cu^{2+} ions in aqueous circumstances selectively and sensitively, we made use of TWNCNDs by making use of the unusual optical features that they possessed. To evaluated the limit of detection (LOD) for TWNCNDs in the presence of metal ions by using the Stern-Volmer equation. The LOD for Cu^{2+} ions was 0.1 µM, and the detection range was from 0 to 0.5 µM. We demonstrated their adaptability and potential for practical industrial usage beyond their applications in analytical chemistry by using the strong blue emission features of the synthesized TWNCNDs as effective fluorescent ink as marking agents and TWNCNDs/PVA polymeric films in a range of commercial anti-counterfeiting applications.

Graphical Abstract

Keywords Termite wings · Hydrothermal method · Quantum yield · Anti-counterfeiting

✉ Jothi Vinoth Kumar
drjvinoth@gmail.com

✉ I. Neelakanta Reddy
neela.sra@gmail.com

✉ Cheolho Bai
chbai@yu.ac.kr

[1] Department of Food and Nutrition, Bio Nanocomposite Research Center, Kyung Hee University, Seoul 02447, Republic of Korea

[2] Department of Chemical Engineering, Agni College of Technology, OMR, Thazhambur 603103 Tamil Nadu, India

[3] Department of Chemistry, Sri Eshwar College of Engineering (Autonomous), Coimbatore 641202, India

[4] Department of Chemistry, Centre for Material Chemistry, Karpagam Academy of Higher Education, Coimbatore, Tamilnadu 641 021, India

[5] Department of Physics, Saveetha School of Engineering, Saveetha Institute of Medical and Technical Sciences (SIMATS), Thandalam, Chennai 602 105, India

[6] Department of Chemistry, College of Science, King Saud University, P. O. Box 2455, Riyadh 11451, Saudi Arabia

[7] School of Mechanical Engineering, Yeungnam University, Gyeongsan, South Korea

Highlights

- A simple hydrothermal approach to create nitrogen-doped carbon nanodots (TWNCNDs) from termite wings.
- The TWNCNDs have high fluorescence (FL) quality with a quantum yield of 11.8%.
- The LOD for Cu^{2+} ions was 0.1 µM, and the detection range was from 0 to 0.5 µM.
- TWNCNDs/PVA polymeric films in a range of commercial anti-counterfeiting applications.

1 Introduction

Heavy metal ions are widely recognized as non-biodegradable micropollutants that accumulate in various environmental compartments, including water bodies and living organisms. Copper, arsenic, lead, iron, cadmium, mercury, and chromium are well-known heavy metal ions, even at trace levels, and they pose significant risks to both human health and environmental integrity. These pollutants are predominantly found in the effluents of industries such as pigment production, acid battery manufacturing, alloy production, printing, herbal product formulation, ceramic and glass production, coating processes, and metal plating [1–4]. Several techniques have been used to detect heavy metal ions, including spectrophotometry, atomic absorption spectroscopy, electron paramagnetic resonance, electrochemical approaches, and other substances such as organic dyes, nanoclusters, metal oxides, and nanodots [5–7]. However, many of these methods suffer from significant drawbacks, including time-consuming procedures.

Counterfeiting is a global issue with serious implications for government bodies, businesses, educational institutions, and consumers. Counterfeit products, spanning commercial goods, microelectronics, automotive components, pharmaceuticals, and official documents, have proliferated in recent years. Carbon nanodots, also known as CNDs, have a bright fluorescence, low cytotoxicity, high quantum yields, and a wide variety of sources, all of which make them very attractive for use in anti-counterfeiting applications. Surprisingly, there is a paucity of study regarding the anti-counterfeiting capability of TWNCNDs (Termite Wing-derived Nitrogen-doped Carbon Nanodots) as luminous materials [8].

Fluorescent nanomaterials have gained prominence due to their rapid detection capabilities, high specificity, solubility, biocompatibility, and ease of use. Semiconductor-based fluorescent quantum dots (FQDs) are frequently employed in metal ion sensing due to their exceptional optical properties. However, FQDs often suffer from toxicity concerns, even at low concentrations, limiting their applicability. Consequently, efforts have been made to develop biocompatible fluorescent QDs. The CNDs are a unique class of zero-dimensional carbon-based nanomaterials with outstanding optical properties suited for a wide range of applications, including optoelectronics, bioimaging, catalysis, and numerous sensor types [9]. Among fluorescent materials, CNDs are the most cost-effective, efficient, and environmentally friendly and have been found to be extensively useful as sensor probes. Various synthesis methods, including laser ablation, electrochemical oxidation, chemical oxidation, arc discharge, hydrothermal, and microwave techniques, have been employed to produce CNDs [10]. Green technology has recently emerged for CND synthesis, offering higher quantum yields, cost-effectiveness, and environmental friendliness. These natural product-derived CNDs, mainly composed of carbon, oxygen, nitrogen, hydrogen, and sulfur, undergo polycondensation to yield CNDs with abundant surface functional groups [11]. Doping with elements like nitrogen, sulfur, boron, chlorine, and phosphorus is commonly employed to enhance fluorescence characteristics, electron transport, and quantum yields. Nonmetal doping can also lead to shifts in the valence and conduction band positions of carbon nanodots. However, there remains a need for novel approaches to create CNDs with high quantum yields and tailored surface functionalization for specific applications [12].

Termite wings are readily available and abundant in nature, making them a convenient and cost-effective source material for the synthesis of quantum dots. Their accessibility ensures a sustainable and eco-friendly approach to nanoparticle production. Termite wings contain chitin, a natural polysaccharide found in the exoskeletons of insects [13, 14]. Chitin serves as a biocompatible and biodegradable precursor for the synthesis of quantum dots, facilitating the green synthesis process. Chitin-rich biomaterials like termite wings possess inherent chemical reactivity due to functional groups present in their composition. These functional groups can serve as reducing and capping agents during the synthesis of quantum dots, promoting the nucleation and growth of nanoparticles [15, 16]. The unique microstructure of termite wings, including their size, shape, and surface features, may influence the nucleation and growth kinetics of quantum dots [15]. By leveraging these natural properties, researchers can potentially achieve control over the size, morphology, and optical properties of the synthesized nanoparticles [17]. Additionally, the use of renewable biomaterials aligns with sustainable practices and reduces the environmental impact associated with nanoparticle synthesis.

In this investigation, we synthesized luminous TWNCNDs by using a conventional hydrothermal

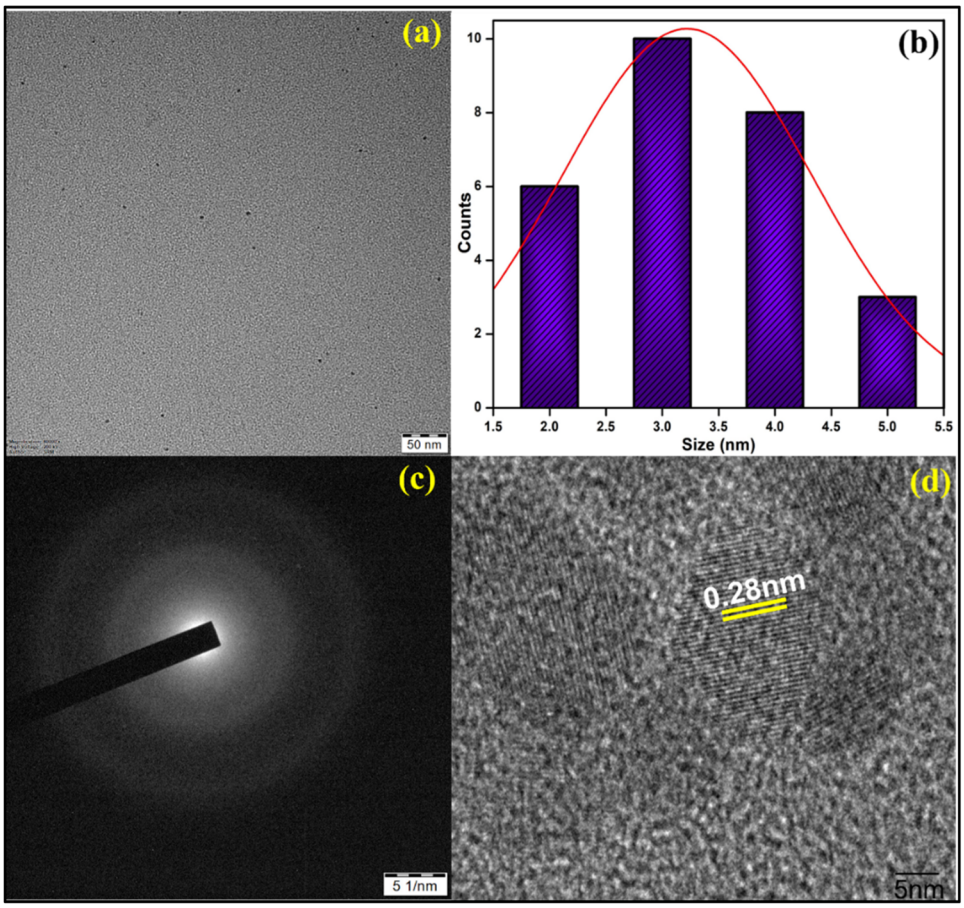

Fig. 1 **a** TEM image of TWNCNDs. **b** Size distribution graph of TWNCNDs. **c** SAED pattern of TWNCNDs. **d** HR-TEM image of TWNCNDs

procedure, with termite wings serving as the carbon source and aqueous ammonia playing the role of the nitrogen dopant. In order to characterize the TWNCNDs that we synthesized, we relied heavily on important spectroscopic techniques. These TWNCNDs emit a strong blue fluorescence and have the ability to selectively, visually, and accurately detect Cu^{2+} ions even when other metal ions are also present. TWNCNDs have the potential to function as powerful anti-counterfeiting agents thanks to their remarkable fluorescence qualities.

2 Result and discussion

2.1 Morphology analysis of TWNCNDs

We performed a thorough characterization of the pristine TWNCNDs, using a variety of approaches to elucidate their structural and morphological characteristics. The TEM analysis unequivocally verified the uniform dispersion of the synthesized TWNCNDs, showcasing their consistent morphology with an average size of 3.3 nm (refer to Fig. 1a, b). The SAED pattern, as depicted in Fig. 1c, exhibited concentric circular rings and a conspicuous bright spot. These features strongly indicate the graphitic structure inherent to TWNCNDs [18, 19]. Furthermore, a high-resolution TEM image (Fig. 1d), corresponding to the (100) crystal facet of graphitic carbon, unveiled well-defined lattice fringes with an interplanar spacing of 0.28 nm. These comprehensive findings collectively underscore the precise structural and morphological characteristics of the TWNCNDs, offering valuable insights into their fundamental properties.

2.2 UV–Vis and FT-IR analysis of TWNCNDs

The UV-vis absorption spectrum of TWNCNDs is thoughtfully presented in Fig. 2a for your examination. This spectrum reveals the presence of two distinctive absorption peaks, each conveying essential information about the nanodots' molecular composition. The first and more prominent absorption peak, observed at 272 nm, can be confidently attributed to the $\pi-\pi^*$ transition of the C = C bonds nestled within the aromatic rings. This resonance provides valuable insights into the nanodots' aromatic structural elements. The second discernible peak, situated at 324 nm, aligns with the n-π^* transitions associated with C = O bonds. Remarkably, these transitions are intimately linked

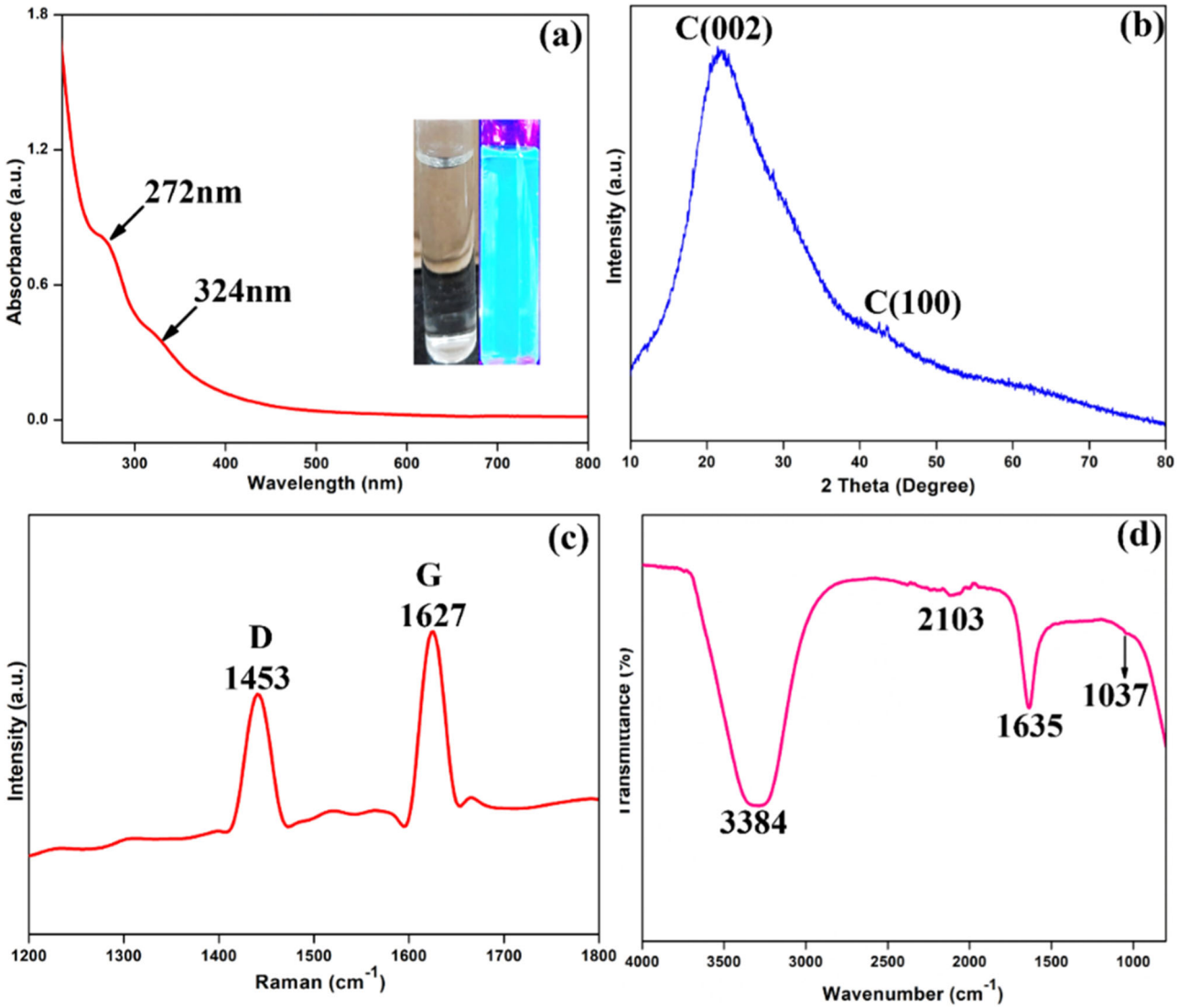

Fig. 2 **a** UV–Visible absorbance spectrum of TWNCNDs. **b** XRD pattern of TWNCNDs. **c** Raman spectrum of prepared TWNCNDs. **d** FTIR spectra of TWNCNDs

to the $\pi-\pi^*$ transition of the C = C bonds found within the aromatic rings, further highlighting the intricate interplay of molecular constituents within the TWNCNDs [20]. When a diluted solution of TWNCNDs in water is exposed to daylight, it appears with a typical color. However, when subjected to UV light at 365 nm, it undergoes a striking transformation, turning vividly blue, as illustrated in the inset of Fig. 2a. This change confirms the successful synthesis of TWNCNDs from termite wings, as corroborated by the UV-Vis data [21].

In terms of structural analysis, we investigated the Raman spectra of TWNCNDs. The D bands observed in the spectra arise from the presence of dangling carbon-atom bonds on disordered graphite termination planes. Conversely, the G bands are associated with the vibration of sp^2 carbon atoms in hexagonal lattices in two dimensions (2D). For TWNCNDs, the ratio of I_D to I_G values was determined to be 0.98, with the intensity of I_D being smaller than that of I_G (I_D/I_G). These findings indicate the presence of a mild graphitic structure in the synthesized TWNCNDs and suggest the existence of minor imperfections on the surface of TWNCNDs' graphitic structure.

Furthermore, we employed FT-IR spectroscopy to delve into the spectrum of functional groups adorning the surface of TWNCNDs. As elucidated in Fig. 2d, the results of this analysis provide critical insights into the molecular composition of these nanodots. A discernible peak at 3384 cm^{-1} signifies the presence of bending vibrations characteristic of O-H bonds, underscoring the involvement of hydroxyl groups on the TWNCND surface. Simultaneously, a peak observed at 2103 cm^{-1} corresponds to the stretching vibrations associated with N-H bonds, a pivotal revelation

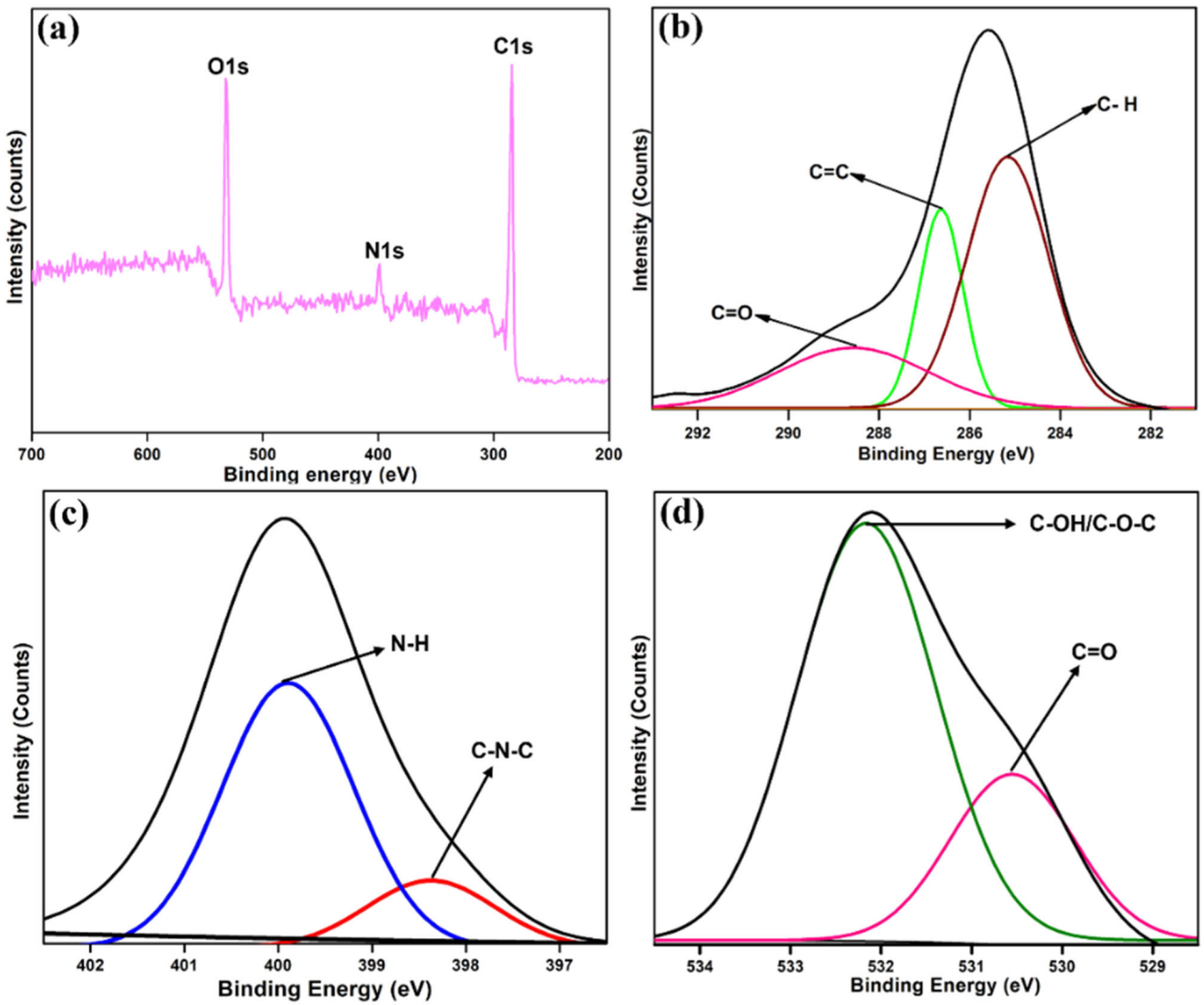

Fig. 3 **a** XPS full spectrum, (**b**) C 1 s spectrum, (**c**) N 1 s spectrum, (**d**) O1s spectrum of the TWNCNDs

indicative of amino (NH_2) groups. Notably, the stretching vibrations originating from C = C/C = O bonds manifest as absorption maxima within the 1635 cm^{-1} range, while those from C-O bonds are distinctly evident at 1037 cm^{-1}. These findings offer compelling evidence of a high concentration of -NH_2 and -COOH functional groups prominently adorning the exterior of TWNCNDs [22, 23].

In Fig. 3a, the comprehensive X-ray photoelectron spectroscopy (XPS) spectra exhibit three distinct peaks situated at 283.6, 399.1, and 532.4 eV, aligning with C1s, N1s, and O1s, respectively. The high-resolution C1s spectra (Fig. 3b) unveil four prominent peaks located at 285.1, 286.6, and 288.4 eV. These peaks can be attributed to specific chemical bonds: C-H bonds, C = C bonds, and C = O bonds, respectively [24]. Figure 3c, the N1s spectra manifest two discernible peaks, one at 398.3 eV and the other at 399.6 eV. These peaks correspond to N-H and C-N-C bonds, respectively, underlining the nitrogen-containing functional groups present on the TWNCNDs' surface. Notably, these surface components detected by XPS are in close agreement with the findings derived from FTIR spectroscopy [25]. Figure 3d provides further elucidation with the O1s spectrum, which can be effectively deconvoluted into two distinctive peak positions at 531.4 and 532.9 eV. These positions align with C = O and C-OH/C-O-C functionalities, respectively, as illustrated in the figure. These XPS data serve as pivotal evidence of the chemical composition of TWNCNDs, conclusively confirming the presence of specific functional groups on their surface.

The optical properties of TWNCNDs are explored using their PL spectra. The as-prepared TWNCNDs had optimal excitation and emission peak wavelengths of 305 nm and 410 nm, respectively (Fig. 4a). They can also exhibit blue

fluorescence when exposed to 365 nm UV light. Figure 4b shows an example of excitation-dependent PL activity. When the excitation wavelength is increased from 345 to 415 nm, the emission evolves to a longer wavelength region with a significant decrease in intensity. The quantum yield of TWNCNDs is 11.8% [26].

2.3 Metal ion sensing capability of TWNCNDs

TWNCNDs are promising for sensing applications because their oxygen-containing surface groups might potentially interact with transition metal ions [27]. We investigated the feasibility of employing TWNCNDs as fluorescence probes for the quantitative measurement of metal ions. As depicted in Fig. 5a, b, an increase in the concentration of Cu^{2+} ions led to a gradual reduction in fluorescence intensity [28]. Figure 5c demonstrates a linear relationship ($R^2 = 0.9897$) within the concentration range of 10 to 70 nM, with a detection limit of 0.1 µM established using the 3 σ/slope method. Various methods to detect Cu^{2+} ions in earlier reports, shown in Table 1.

In order to comprehensively investigate the influence of diverse metal ions on TWNCNDs, we conducted an extensive examination of fluorescence intensities both in the presence and absence of specific metal ions. The selected metal ions encompassed a wide range, including Co^{2+}, Cu^{2+}, Ba^{2+}, Fe^{3+}, Ag^{+}, Pb^{2+}, Cr^{3+}, Mg^{2+}, Zn^{2+}, Hg^{2+}, Mn^{2+}, Cr^{6+}, Ca^{2+}, and K^{+}. Remarkably, only the addition of Cu^{2+} induced an instantaneous and significant decrease in fluorescence intensity when introduced to the untreated TWNCNDs (Fig. 5d). In contrast, introducing other metal ions resulted in negligible or no noticeable alterations in fluorescence intensity. This observed fluorescence quenching phenomenon provided strong evidence for the selectivity of TWNCNDs toward Cu^{2+} ions. The mechanism underlying fluorescence quenching involves electron or energy transfer mediated by functional groups present on the surface of TWNCNDs. We further explored the sensitivity of this system to Cu^{2+} ions by examining the variations in fluorescence intensity with increasing Cu^{2+} concentration [29]. The study involved monitoring changes in fluorescence intensity after adding varying amounts of Cu^{2+} to a fixed concentration of TWNCNDs solution upon excitation at 305 nm. The results underscored the potential utility of TWNCNDs as a sensitive and selective probe for the quantification of Cu^{2+} ions.

2.4 Interfering analysis of TWNCNDs

In the study conducted, the selectivity of TWNCNDs as a fluorometric sensor was assessed by examining the emission responses in the presence of various competitive metal ions. The investigation aimed to evaluate the sensor's ability to detect Cu^{2+} ions amidst other potentially interfering ions selectively [28]. The emission responses were studied under optimum conditions. The Cu^{2+} ions at a concentration of 70 nM were introduced into a TWNCNDs dispersion containing other competitive ions 80 nM. The emission spectra were recorded and analyzed to observe any changes in the emission intensity. The emission intensity corresponding to Cu^{2+} ions was observed to decrease, indicating quenching, as these ions formed complexes with the sensing probe [30]. The influence of other competitive ions on the emission band was investigated at higher concentrations 80 nM. Surprisingly, the presence of other competitive ions had an insignificant effect on the emission band, even at higher concentrations as shown in Fig. 6. The investigation revealed that TWNCNDs exhibited high

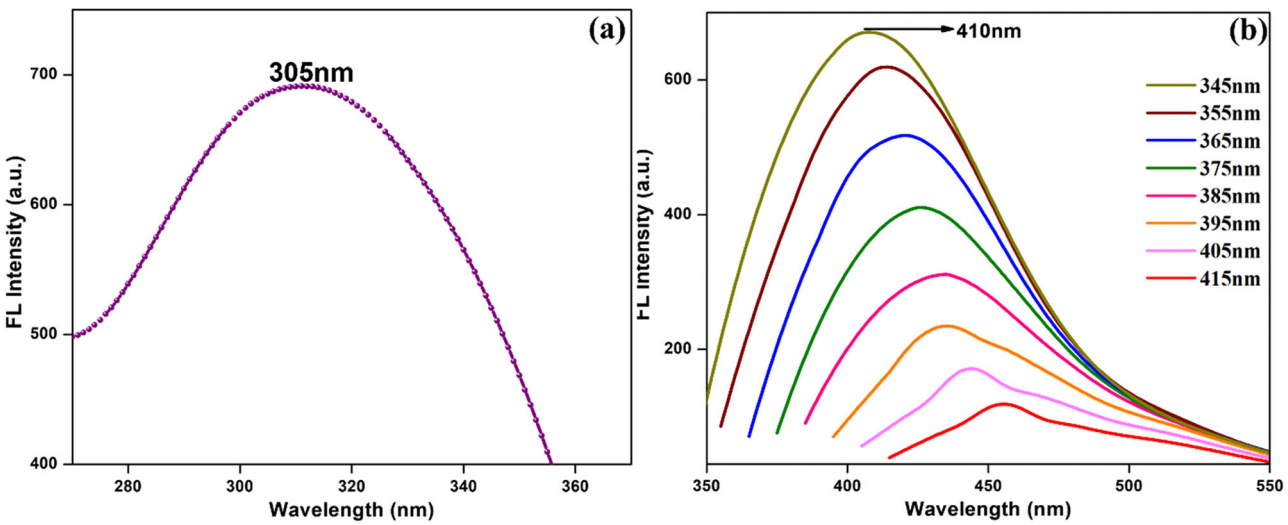

Fig. 4 **a** The excitation spectra of TWNCNDs, (**b**) different excitation wavelengths

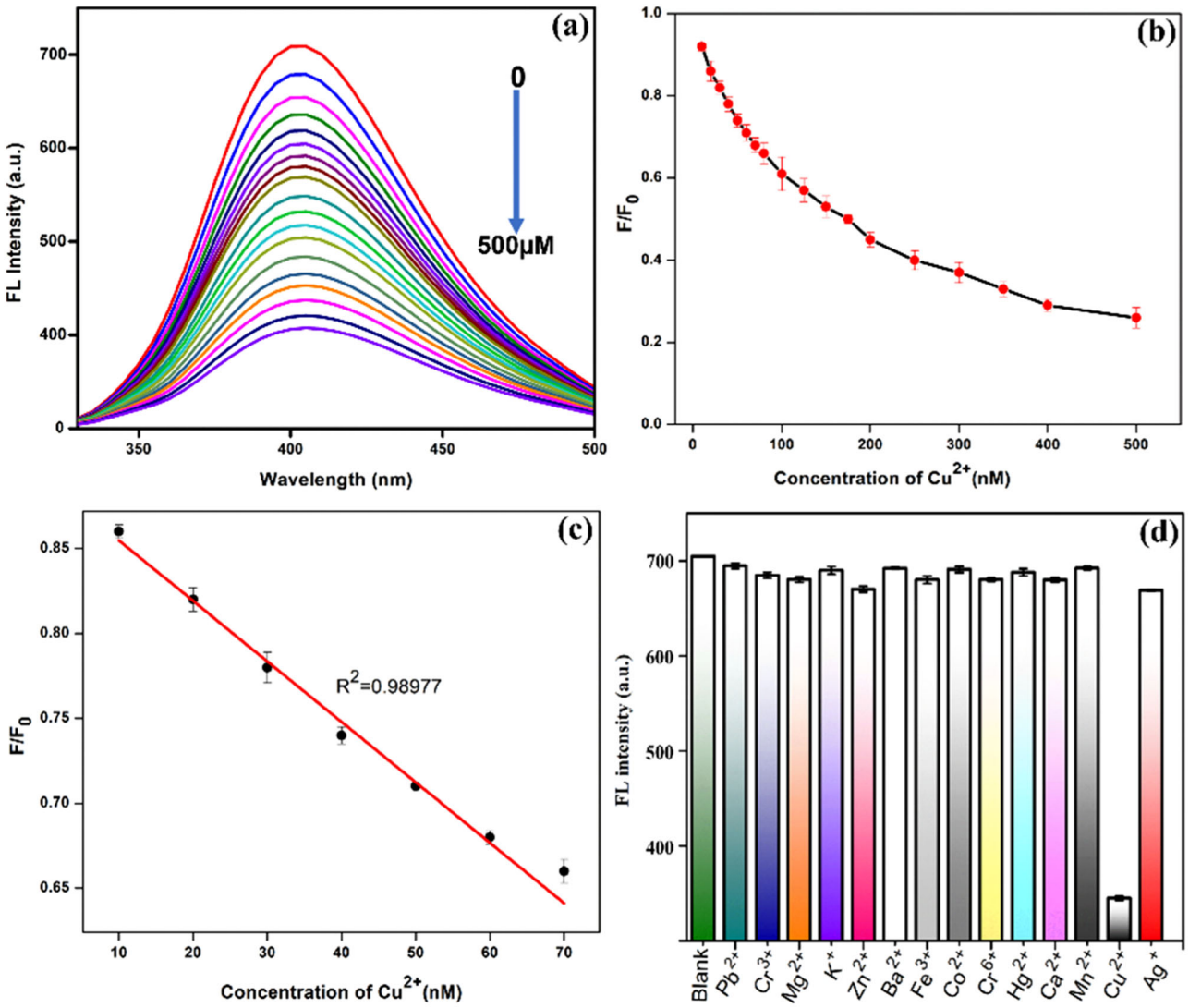

Fig. 5 **a** Fluorescence spectra for Cu^{2+} TWNCNDs, at various concentrations (10, 20, 30, 40, 50, 60, 70, 80, 100, 125, 150, 175, 200, 250, 300, 350, 400, and 500 nM) in 20 mM Tris (pH = 7.5) at 37 °C; (**b**) Fluorescence resolution versus Cu^{2+} concentrations; (**c**) linear relationship among fluorescence intensity and Cu^{2+} concentrations (10–70 nM); (Surprisingly, there is a paucity of study regarding the anti-counterfeiting). **d** Cu^{2+} selectivity versus coexisting metal ions. The standard deviation is displayed by the error bars for three different tests

Table 1 Comparison of different fluorescent probes for sensing Cu^{2+}

Methods	Detection range(μM)	Detection limit(μM)	References
Fluorescence	0–8	0.29	[41]
Fluorescence	0–50	0.001	[42]
Electrochemistry	0.3–1.4	0.3	[43]
Colorimetry	0.1–10	0.5	[44]
Fluorescence	10–150	3.5	[45]
Colorimetry	0.25–14	0.25	[46]
Colorimetry	0.625–15	0.29	[47]
Fluorescence	0–0.5	0.1	This work

selectivity and specificity towards Cu^{2+} ions over other metal ions. This study underscores the importance of understanding the selectivity profile of sensing materials, particularly in environmental monitoring applications, where accurate detection of specific ions is crucial for public health and safety.

2.5 Quenching mechanism

In dealing with fluorescent materials in the presence of quenchers, it's important to understand the two primary mechanisms of fluorescence quenching: dynamic quenching and static-ground state quenching [31]. Dynamic quenching

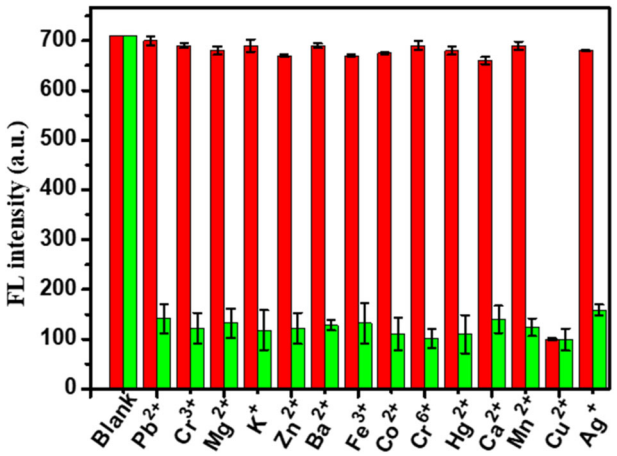

Fig. 6 Interference experiments of other metal ions

involves introducing the quencher into the fluorescent material solution, where it quickly diffuses and mixes with the fluorescent molecules. As a consequence, the intensity of the fluorescence diminishes following irradiation. This decrease in fluorescence intensity occurs due to the frequent collisions between the excited state fluorescent molecules and the quencher [32]. Think of it as the quencher "stealing" the energy from the excited fluorescent molecules, causing them to return to their ground state and emit fewer photons. Importantly, the degree of fluorescence quenching in dynamic quenching is influenced by the concentration of the quencher; when there's a higher concentration of quencher molecules, there are more collisions, leading to more pronounced fluorescence quenching. This process is inherently time-dependent, with the rate of quenching related to the diffusion rate of the quencher molecules. On the other hand, static quenching involves a slightly different mechanism. In this scenario, the quencher interacts with the fluorescent material through chemical bonding, forming a complex. This complexation process results in certain fluorescent molecules becoming less susceptible to irradiation effects [33]. When the complex is excited by irradiation, it does not emit photons as it returns to the ground state. This is because energy from the excited state is utilized in the formation of new coordinate chemical bonds within the complex, effectively "locking" the energy and preventing its release as fluorescence [34, 35].

Consequently, static quenching reduces the intensity of fluorescence due to these chemical interactions between the quencher and the fluorescent material. Finally, both dynamic and static quenching mechanisms lead to a reduction in fluorescence intensity, but they do so through different processes. Dynamic quenching relies on collisions and energy transfer between the quencher and fluorescent molecules, while static quenching involves the formation of stable complexes and the subsequent inhibition of fluorescence emission due to chemical bonding within the complex. Understanding these mechanisms is crucial for interpreting and utilizing fluorescence quenching phenomena in various applications, including in your research.

2.6 Fluorescent ink application of TWNCNDs

Counterfeiting is a global issue with significant implications for governments, businesses, and consumers. Consequently, there is a pressing need for the development of anti-counterfeiting agents that facilitate the straightforward identification of counterfeit items such as currency, passports, official documents, and certificates [36]. The synthesized TWNCNDs display distinct fluorescence characteristics that hold immense practical value in real-world anti-counterfeiting applications. This field encompasses diverse materials, including carbon dots, rare-earth metals, polymer dots, perovskite materials, and metal-based nanoparticles. For instance, carbon dots offer advantages such as excellent dispersibility, non-toxicity, environmental friendliness, and cost-effectiveness. In the case of TWNCNDs, we employed polyvinyl alcohol (PVA) as the polymer matrix due to its numerous merits, including high hydrophilicity, biocompatibility, optical transparency, and ease of processing. Additionally, -OH groups within PVA's molecular structure facilitate hydrogen bonding, enhancing the traceable UV-light recovery response [37]. To illustrate, we created "Letters" using a mixture of TWNCNDs and polyvinyl alcohol (PVA), which could be directly utilized as ink. These letters were allowed to air dry at room temperature, as depicted in Fig. 7a. In the open air, the low TWNCNDs mixture (0.15 wt%) appears colorless; however, it exhibits robust blue fluorescence when exposed to a 365 nm UV lamp (Fig. 7b). The fluorescent ink derived from TWNCNDs presents a cost-effective raw material and a straightforward synthesis process, rendering it a promising candidate for producing fluorescent inks. This innovation has paved the way for the effective utilization of synthetic TWNCNDs as a potent anti-counterfeiting agent.

2.7 Polymeric film for anti-counterfeiting

The TWNCNDs/PVA polymeric film has been proven as a suitable lighting material for advanced prevention of counterfeiting (AC) applications. When exposed to 365 nm UV light, this flexible polymeric flim material enables for secure and convenient information encryption and decryption, making it an excellent method of protecting sensitive data [38]. We can see that the synthesized TWNCNDs/PVA polymeric films have high optical transparency and are brightly luminous with various hues when exposed to ultraviolet light (Fig. 8a). The model picture may be seen quite clearly under the produced anti-counterfeit fluorescent

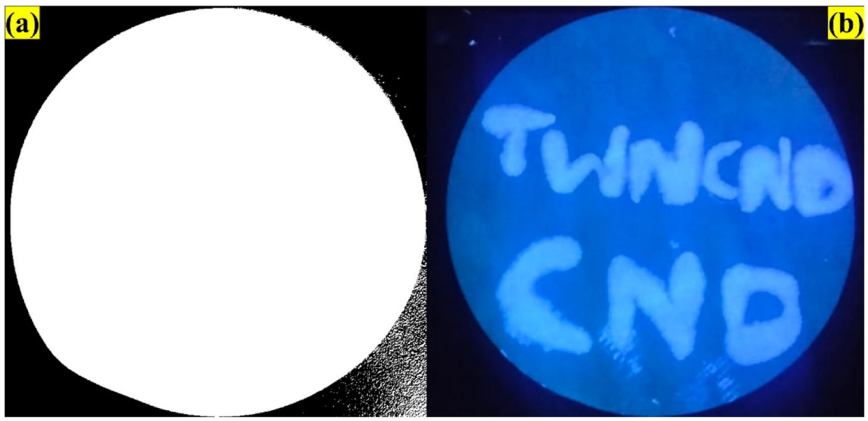

Fig. 7 Fluorescent ink Patterning agents are (**a**) under daylight and (**b**) under UV light

polymeric film. TWNCNDs/PVA polymeric films exhibit blue fluorescence when exposed to UV light at 365 nm. We run a 60-day storage test to see how stable the TWNCNDs/PVA polymeric film [39]. Despite this extended interval (Fig. 8c), the emission color of the AC pattern remained constant. This strong and continuous blue emission demonstrates the ecological resilience of TWNCNDs/PVA, confirming its applicability for security applications. These findings give solid evidence that the TWNCNDs/PVA polymeric film is effective and durable in security applications. In Fig. 8b, d show photographic views of TWNCNDs/PVA films under various folds, illustrating their potential for a wide range of applications in the field of flexible electronics. This visual evidence demonstrates that when exposed to UV 365 nm excitation light, they create a vibrant blue glow, demonstrating that PVA does not impair TWNCNDs' exceptional performance in photoluminescence tests. To broaden their applications, we combined TWNCNDs generated from an abundant and non-toxic source with PVA to form flexible and transparent polymeric films [40]. Bare PVA films were also tested without the addition of TWCNDs UV and naked eye films, as shown in Fig. 8. This technology has promise for lifting and detecting long-term exposed anti-counterfeiting applications. Furthermore, the materials utilized are widely available and safe. This study demonstrates the efficacy of interfacial segregation of TWNCNDs in polymer films, which opens up new possibilities for a variety of applications.

3 Conclusions

In conclusion, we found that a simple hydrothermal procedure can be used to manufacture heteroatom-doped carbon nanodots, and our research supports this finding. Termite wings were used as a carbon source, and ammonia solution was used as a nitrogen source. Extensive studies with XPS and FT-IR confirmed the efficient surface functionalization of carbon nanodots (TWNCNDs) with nitrogen heteroatoms. An XRD analysis revealed that the synthesized TWNCNDs were both amorphous and graphitic, with a spherical shape and an average particle size of 3.3 nm. The research results corroborated these observations. The unique optical characteristics of TWNCNDs were determined by fluorescence and UV-Vis spectroscopy. The detection of Cu^{2+} ions in aqueous solutions was made much simpler and more effective by employing a fluorescence-based approach, and TWNCNDs were utilized as the fluorescence probe. This method has an excellent detection limit of 0.1 µM and a linear detection range from 0 to 0.5 µM. Two types of fluorescence-suppressing mechanisms, one dynamic and one static, helped to promote the interaction between TWNCNDs and Cu^{2+} ions. The detection of Cu^{2+} ions in real samples was tested and found to be successful, validating the practical use of our technology. As a bonus, TWNCNDs have been successfully used as fluorescent ink for anti-counterfeiting purposes, where they have proven to be an effective, safe, and low-cost solution. As a result of their wide range of potential uses, TWNCNDs have recently gained attention as a promising choice for a fluorescence probe. Finding and lifting anti-counterfeiting apps that have been exposed for a long time is a potential use case for this technology. Additionally, the materials utilized are both easily accessible and non-toxic. The paper highlights the effective separation of TWNCNDs in polymer films, which can be used for multiple applications.

4 Experimental section

4.1 Materials and methods

Every metal salt was of analytical grade including Calcium nitrate tetrahydrate $Ca(NO_3)_2.4H_2O$, Mercuric nitrate $Hg(NO_3)_2.H_2O$, Lead(II) nitrate $Pb(NO_3)_2$, Palladium(II) nitrate $Pd(NO_3)_2.2H_2O$, Manganese(II) nitrate $Mn(NO_3)_2.4H_2O$, Zinc nitrate $Zn(NO_3)_2$, Rhodium(III)

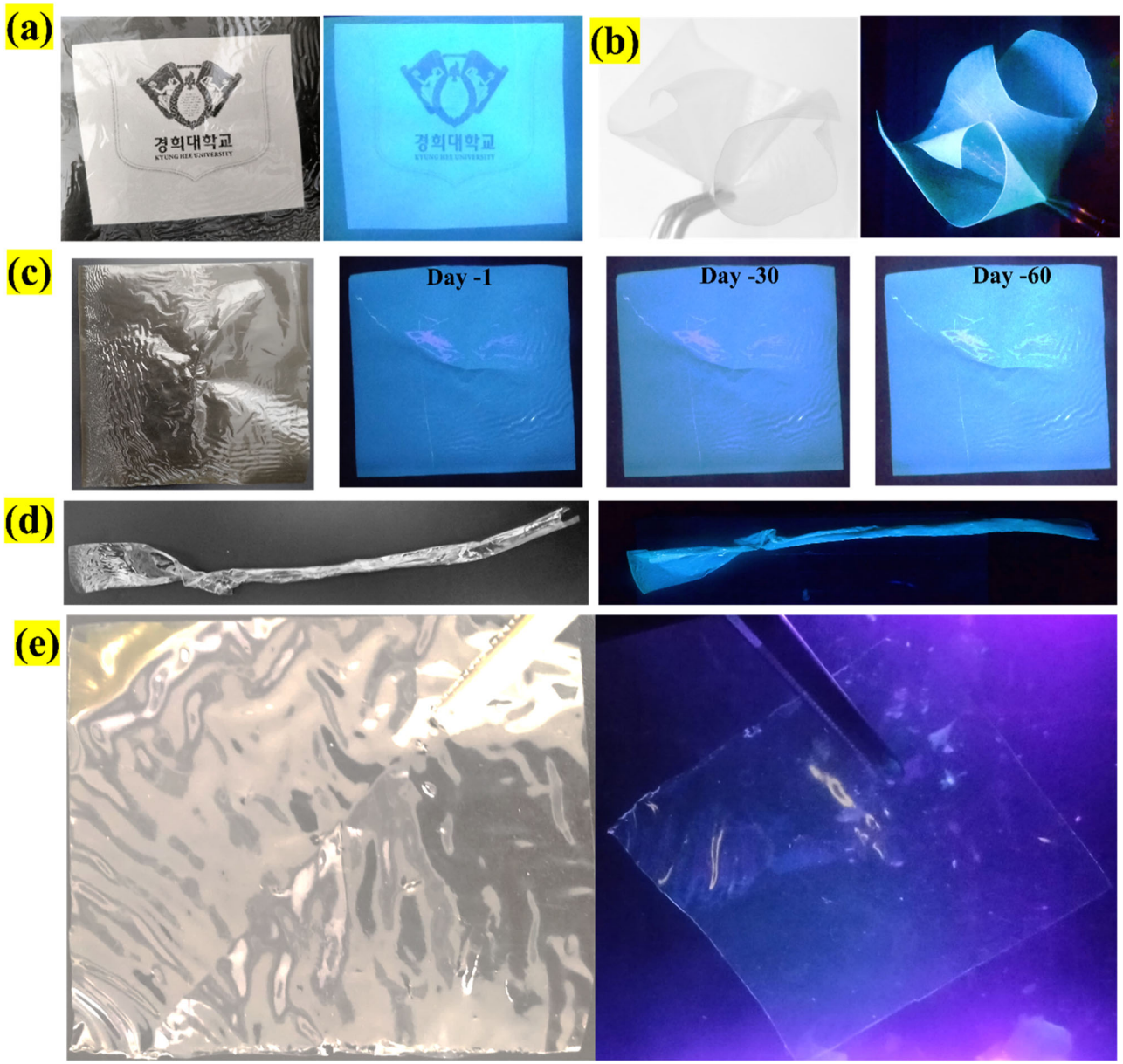

Fig. 8 **a** The light transmission of the developed TWNCNDs/PVA polymeric films, (**b**) The TWNCNDs/PVA polymeric films are very flexible and easy to fold when exposed to UV 365 nm light, (**c**) TWNCNDs/PVA polymeric films aged up to 60 days, (**d**)Twisted films of TWNCNDs/PVA, (**e**) Without TWNCNDs in PVA polymeric films naked eye(left) and UV light(right)

nitrate hydrate $Rh(NO_3).H_2O$, Nickel(II) nitrate hexahydrate $Ni(NO_3).6H_2O$, Iron(III) nitrate $Fe_2(NO_3).9H_2O$, Copper(II) nitrate trihydrate $Cu(NO_3)_2.3H_2O$, Arsenic trichloride $As(Cl)_3$, Platinum(IV) Nitrate $Pt(NO_3)_4$, Silver nitrate $Ag(NO_3)$, Selenium dioxide SeO_2, Cadmium nitrate tetrahydrate $Cd(NO_3)_2.4H_2O$, Ammonium Molybdate $(NH_4)_6Mo_7O_{24}$, Cobalt(II) nitrate $Co(NO_3)_2.6H_2O$, Aluminium Nitrate $Al(NO_3)_3.9H_2O$, Chromium Nitrate $Cr(NO_3).9H_2O$, were obtained from avara chemicals. Quinine sulfate as a fluorescence standard reference (98%) was obtained from loba chemicals. Every experiment utilized deionized water.

4.2 Synthesis of TWNCNDs

A specific quantity of termite wings extract (50 mL) was combined with ammonia, then heated at 200 °C for 6 h in a high-pressure reactor for 2 h. The dark-brown mixture was dissolved in deionized water after allowing it to cool to room temperature. After 30 min of vigorous stirring using a magnetic agitator and 10 min of centrifugation at 12,000 rpm to eliminate larger particles, the resultant solution exhibited a dark-brown hue. Subsequently, this solution underwent activation dialysis, employing a molecular weight cutoff bag of 3000 Da, for a duration of 48 h. The

outcome of this process was a clear, light brown solution, which was then meticulously labeled as TWNCNDs and appropriately stored at a temperature of 4 °C for further use in our research study.

4.3 Fluorescent quantum yield measurement

To determine the quantum yield (QY) of the TWNCNDs, we conducted a comparison between their absorbance values and integrated photoluminescence intensities in relation to a reference substance, quinine sulfate [17]. Quinine sulfate, known to have a quantum yield (QY) of 0.54, was dissolved in a 0.1 M H_2SO_4 solution, whereas the carbon dots (CDs) were being dispersed throughout the distilled water. The calculation for quantum yield (Φ) is expressed as follows:

$$\Phi = \Phi R \times I/IR \times AR/A \times \eta^2/\eta^2 R \quad (1)$$

Here, Φ represents the quantum yield of the TWNCNDs, I is the integrated emission intensity, A is the optical density (OD), and η is the refractive index. This equation allows us to quantitatively assess the quantum yield of the TWNCNDs by comparing their fluorescence properties to those of the reference quinine sulfate.

4.4 Characterization of TWNCNDs

During the course of our study, an extensive array of spectroscopic techniques was employed to characterize the materials under investigation comprehensively. Ultraviolet-visible (UV-vis) spectra were acquired at room temperature using a Jasco UV3600 spectrophotometer, a reputable instrument crafted by Jasco. For fluorescence spectra, we utilized a spectrofluorometer from the same manufacturer, featuring a 10 mm optical path quartz cell and covering a wavelength range of 300–600 nm. The excitation wavelength was systematically varied, incrementally stepping from 290 nm to 360 nm. Fourier-transform infrared (FT-IR) spectra were obtained utilizing a Thermo-manufactured spectrometer, known as the Nicolet 380. In parallel, an X-ray diffractometer (PANalytical Empyrean) was employed to scrutinize the patterns resulting from powder X-ray diffraction (XRD). X-ray photoelectron spectra (XPS) were meticulously collected using a Shimadzu-manufactured spectrometer named the Kratos AXIS SUPRA. These analyses provided invaluable insights into the materials' elemental composition and chemical states. To delve deeper into the microstructural characteristics, investigations through transmission electron microscopy (TEM) were conducted at room temperature. These examinations were carried out with the aid of a JEOL JEM-1010 transmission electron microscope. The utilization of this diverse array of spectroscopic and microscopic techniques enabled us to thoroughly elucidate the properties of the materials under scrutiny, providing essential insights that significantly contributed to the depth and comprehensiveness of our research.

4.5 Detection for Cu^{2+}

In our experimental setup, we conducted Cu^{2+} measurements at room temperature (RT) in a PBS buffer solution with a pH of 3.5 and a concentration of 0.1 M. Typically, we filled a 3 mL fluorescence cuvette with 100 µL of TWNCNDs at a concentration of 1 mg/L, added 40 µL of PBS buffer solution, and introduced the corresponding Cu^{2+} standard solution. The volume was adjusted to a constant 3 mL by adding distilled water. After observing the process for 8 min, we recorded the fluorescence spectra at 305/410 nm for excitation and emission, respectively. The signal output value was determined by taking the difference between the fluorescence intensity of TWNCNDs in the absence of Cu^{2+} (F_0) and in the presence of Cu^{2+} (F) and dividing by F_0. Competing metals were also tested using this method.

4.6 Fluorescent ink of TWNCNDs

Fluorescent ink was made by combining a 10 mL solution of synthetic TWNCNDs with a polyvinyl alcohol (PVA) suspension at a concentration of 10%. After 30 min of magnetic stirring, the PVA was dissolved and the ink's viscosity was increased. The resulting ink was poured into a dry pen cartridge and used to make notes on office paper. After that, it was exposed to UV light analysis after being air-dried at ambient temperature.

4.7 Flexible TWNCNDs/PVA polymer films

To make the TWNCNDs/PVA polymer matrix, first mix 15 g PVA crystals along with 5 mL TWNCNDs and 100 ml of deionized water (DI) in a three-necked, round-bottomed flask with a magnetic stirrer. The mixed solution was agitated at 60 °C for 4 h to ensure that the added fillers were evenly distributed throughout the polymer matrix. The solution mixture (105 mL) was cast over a glass plate coated with Teflon film (30 cm × 24 cm) for 72 h at 28 °C. The dried films were carefully peeled and stored in the humidity chamber (model FX 1077, Jeio Tech Co. Ltd., Ansan, Korea) at 25 °C and 50% relative humidity for 48 h before further study.

Acknowledgements The work was supported by Researchers Supporting Project number (RSPD2024R663), King Saud University, Riyadh, Saudi Arabia.

Author contributions J. Vinoth Kumar, I. Neelakanta Reddy, Cheolho Bai: Conceptualization, Investigation, Writing-original draft, Methodology, Resources, Writing - review & editing. Duraisamy Karthika, V. Arul, K. Radhakrishnan, Pitcheri Rosaiah: Formal analysis. Samar A. Aldossari: Investigation.

Compliance with ethical standards

Conflict of interest The authors declare no competing interests.

References

1. Rudd ND, Wang H, Fuentes-Fernandez EM, Teat SJ, Chen F, Hall G, Chabal YJ, Li J (2016) Highly efficient luminescent metal-organic framework for the simultaneous detection and removal of heavy metals from water. ACS Appl Mater Interfaces 8(44):30294–30303
2. Kumar JV, Alam MW, Selvaraj M, Almutairi HH, Albuhulayqah M, Sadaf S, Joo SW (2024) Fluorescent carbon dots for biodiesel production: a comprehensive review (2019–2024). Inorg Chem Commun 162:112247
3. Nivetha MS, Kumar JV, Arulmozhi R, Abirami N (2023) Ultrathin 2D type-II heterojunctions ZCLDH/CN with a higher photocatalytic performance of ciprofloxacin under simulated light illumination. Opt Mater 140:113861
4. Wang Z, Xu C, Lu Y, Chen X, Yuan H, Wei G, Ye G, Chen J (2017) Fluorescence sensor array based on amino acid derived carbon dots for pattern-based detection of toxic metal ions. Sens Actuators B Chem 241:1324–1330
5. Kumar JV, Ajarem JS, Allam AA, Manikandan V, Arulmozhi R, Abirami N (2022) Construction of SnO_2/g-C_3N_4 an effective nanocomposite for photocatalytic degradation of amoxicillin and pharmaceutical effluent. Environ Res 209:112809
6. del Castillo Busto ME, Montes-Bayón M, Bettmer J, Sanz-Medel A (2008) Stable isotope labelling and FPLC–ICP-SFMS for the accurate determination of clinical iron status parameters in human serum. Analyst 133(3):379–384
7. Sachin S, Sundaram SJ, Franklin JB, Raj AD, Kumar JV, Alam MW (2024) Synthesis of Zinc Oxide nano bars incorporated with activated Carbon (ZnO NBs/AC) nanocomposites for high specific capacitance value. J Sol-Gel Sci Technol 109:1–9
8. Kumar JV, Arul V, Arulmozhi R, Abirami N (2022) Boron doped fluorescent carbon nano dots for the reduction of ionic dyes and as encryption/decryption QR security code labels. N. J Chem 46(16):7464–7476
9. Arul V, Sampathkumar N, Kotteeswaran S, Arul P, Aljuwayid AM, Habila MA, Govindasamy M (2023) Biomass derived nitrogen functionalized carbon nanodots for nanomolar determination of levofloxacin in pharmaceutical and water samples. Microchim Acta 190(6):242
10. Tammina SK, Jyothi L, Kumar JV, Srivastava H, Naraharisetty SRG (2024) Sensing, detoxification and bactericidal applications of nitrogen-doped carbon dots. Diam Relat Mater 144:111013
11. Nithyabalaji R, Ramya RM, Kavitha R, Radhakrishnan K, Kumar JV, Al-Asbahi BA, Joo SW (2024) Molecular structure, characterization, in vitro and in-silico studies of N, N-dimethyl aminophenyl schiff's base-chalcone hybrid. Chem Phys Impact 8:100422
12. Kumar JV, Rhim JW (2024) Fluorescent carbon quantum dots for food contaminants detection applications. J Environ Chem Eng 12:111999
13. Arul V, Sethuraman MG (2019) Hydrothermally green synthesized nitrogen-doped carbon dots from Phyllanthus emblica and their catalytic ability in the detoxification of textile effluents. ACS omega 4(2):3449–3457
14. Radhakrishnan K, Panneerselvam P, Marieeswaran M (2019) A green synthetic route for the surface-passivation of carbon dots as an effective multifunctional fluorescent sensor for the recognition and detection of toxic metal ions from aqueous solution. Anal Methods 11(4):490–506
15. Kumar JV, Karthika D, Radhakrishnan K, Arul V, Alam MW, Rosaiah P, Joo SW (2013) MXene nanocomposites for current trend applications: synthesis, properties, and future directions. J Mol Liquids 394:123787
16. Vinoth Kumar J, Kavitha G, Arulmozhi R, Arul V, Singaravadivel S, Abirami N (2021) Green sources derived carbon dots for multifaceted applications. J Fluoresc 31:915–932
17. Radhakrishnan K, Sivanesan S, Panneerselvam P (2020) Turn-On fluorescence sensor based detection of heavy metal ion using carbon dots@ graphitic-carbon nitride nanocomposite probe. J Photochem Photobiol A Chem 389:112204
18. Arul V, Radhakrishnan K, Sampathkumar N, Vinoth Kumar J, Abirami N, Inbaraj BS (2023) Detoxification of toxic organic dye by heteroatom-doped fluorescent carbon dots prepared by green hydrothermal method using Garcinia mangostana extract. Agronomy 13(1):205
19. Arul V, Chandrasekaran P, Sivaraman G, Sethuraman MG (2023) Biogenic preparation of undoped and heteroatoms doped carbon dots: effect of heteroatoms doping in fluorescence, catalytic ability and multicolour in-vitro bio-imaging applications-a comparative study. Mater Res Bull 162:112204
20. Jothi VK, Ganesan K, Natarajan A, Rajaram A (2021) Green synthesis of self-passivated fluorescent carbon dots derived from rice bran for degradation of methylene blue and fluorescent ink applications. J Fluoresc 31:427–436
21. Kumar VN, Tamilanban T, Sultana TS, Manasa K, Ragulkumar E, Kumar JV, Arul K (2023) In silico study of traditional Chinese medicinal compounds targeting alzheimer's disease amyloid beta-peptide (1–42). Chem Phys Impact 7:100383
22. Kumar JV, Kavitha G, Albasher G, Sajjad M, Arulmozhi R, Komal M, Nivetha MS, Abirami N (2022) Multiplex heteroatoms doped carbon nano dots with enhanced catalytic reduction of ionic dyes and QR code security label for anti-spurious applications. Chemosphere 307:136003
23. Kumar JV, Tammina SK, Rhim JW (2024) One-step hydrothermal synthesis of sulfur quantum dots for detection of Hg^{2+} ions and latent fingerprints. Colloids Surf A: Physicochem Eng Asp 690:133682
24. Raj SNM, Jothi VK, Rajaram A, Suresh P, Murugan K, Natarajan A (2023) Rational design of α-MnO_2/HT-GCN nanocomposite for effective photocatalytic degradation of ciprofloxacin and pernicious activity. Environ Sci Pollut Res 30:1–19
25. Jia J, Lin B, Gao Y, Jiao Y, Li L, Dong C, Shuang S (2019) Highly luminescent N-doped carbon dots from black soya beans for free radical scavenging, Fe^{3+} sensing and cellular imaging. Spectrochim Acta Part A: Mol Biomol Spectrosc 211:363–372
26. Kumar JV, Kavitha G, Arulmozhi R, Arul V, Abirami N (2021) Cyan color-emitting nitrogen-functionalized carbon nanodots (NFCNDs) from Indigofera tinctoria and their catalytic reduction of organic dyes and fluorescent ink applications. RSC Adv 11(44):27745–27756
27. Shamim SUD, Roy D, Alam S, Piya AA, Rahman MS, Hossain MK, Ahmed F (2022) Doubly doped graphene as gas sensing materials for oxygen-containing gas molecules: a first-principles investigation. Appl Surf Sci 596:153603
28. Bian W, Wang F, Zhang H, Zhang L, Wang L, Shuang S (2015) Fluorescent probe for detection of Cu^{2+} using core-shell CdTe/ZnS quantum dots. Luminescence 30(7):1064–1070

29. Wu YS, Huang FF, Lin YW (2013) Fluorescent detection of lead in environmental water and urine samples using enzyme mimics of catechin-synthesized Au nanoparticles. ACS Appl Mater Interfaces 5(4):1503–1509
30. Sun S, Chen Q, Tang Z, Liu C, Li Z, Wu A, Lin H (2020) Tumor microenvironment stimuli-responsive fluorescence imaging and synergistic cancer therapy by carbon-dot–Cu^{2+} nanoassemblies. Angew Chem 132(47):21227–21234
31. Rohman MA, Baruah P, Bhatta A, Mitra S (2019) Deciphering the interactions of substituted chromones possessing acetylcholinesterase inhibition activity in human serum albumin matrix. J Mol Liq 290:111210
32. Xu S, Chen R, Zheng C, Huang W (2016) Excited state modulation for organic afterglow: materials and applications. Adv Mater 28(45):9920–9940
33. Zhou H, Chua MH, Tang BZ, Xu J (2019) Aggregation-induced emission (AIE)-active polymers for explosive detection. Polym Chem 10(28):3822–3840
34. Rahman M, Harmon HJ (2006) Absorbance change and static quenching of fluorescence of meso-tetra (4-sulfonatophenyl) porphyrin (TPPS) by trinitrotoluene (TNT). Spectrochim Acta Part A: Mol Biomol Spectrosc 65(3-4):901–906
35. Zu F, Yan F, Bai Z, Xu J, Wang Y, Huang Y, Zhou X (2017) The quenching of the fluorescence of carbon dots: a review on mechanisms and applications. Microchim Acta 184:1899–1914
36. Rival JV, Mymoona P, Vinoth R, Mohan AV, Shibu ES (2021) Light-emitting atomically precise nanocluster-based flexible QR codes for anticounterfeiting. ACS Appl Mater Interfaces 13(8):10583–10593
37. Yan L, Yu Y (2019) Rapid and eco-friendly synthesis of red fluorescent gold nanoclusters for sensing and anti-counterfeiting applications. Nano 14(09):1950121
38. Liang C, Shi Q, Zhang Y, Xie X (2023) Water-soluble carbonized polymer dots with tunable solid-and dispersion-state fluorescence for multicolor films, anti-counterfeiting, and fungal imaging. Mater Today Nano 22:100324
39. Jiang W, Liu L, Wu Y, Zhang P, Li F, Liu J, Huang W (2021) A green-synthesized phosphorescent carbon dot composite for multilevel anti-counterfeiting. Nanoscale Adv 3(15):4536–4540
40. Zhang H, Sun L, Guo X, Xu J, Zhao X, Xia Y (2023) Multicolor fluorescent/room temperature phosphorescent carbon dot composites for information encryption and anti-counterfeiting. Appl Surf Sci 613:155945
41. Zhang Y, Li K, Ren S, Dang Y, Liu G, Zhang R, Zhang K, Long X, Jia K (2019) Coal-derived graphene quantum dots produced by ultrasonic physical tailoring and their capacity for Cu (II) detection. ACS Sustain Chem Eng 7(11):9793–9799
42. Liu S, Tian J, Wang L, Zhang Y, Qin X, Luo Y, Asiri AM, Al-Youbi AO, Sun X (2012) Hydrothermal treatment of grass: a low-cost, green route to nitrogen-doped, carbon-rich, photoluminescent polymer nanodots as an effective fluorescent sensing platform for label-free detection of Cu (II) ions. Adv Mater 24(15):2037–2041
43. Xu X, Duan G, Li Y, Liu G, Wang J, Zhang H, Dai Z, Cai W (2014) Fabrication of gold nanoparticles by laser ablation in liquid and their application for simultaneous electrochemical detection of Cd^{2+}, Pb^{2+}, Cu^{2+}, Hg^{2+}. ACS Appl Mater Interfaces 6(1):65–71
44. Miao LJ, Xin JW, Shen ZY, Zhang YJ, Wang HY, Wu AG (2013) Exploring a new rapid colorimetric detection method of Cu^{2+} with high sensitivity and selectivity. Sens Actuators B Chem 176:906–912
45. Yang YZ, Xiao N, Cen YY, Chen JR, Liu SG, Shi Y, Fan YZ, Li NB, Luo HQ (2019) Dual-emission ratiometric nanoprobe for visual detection of Cu (II) and intracellular fluorescence imaging. Spectrochim Acta Part A: Mol Biomol Spectrosc 223:117300
46. Wu X, Gong X, Dong W, Ma J, Chao J, Li C, Wang L, Dong C (2016) A novel fluorescein-based colorimetric probe for Cu^{2+} detection. RSC Adv 6(64):59677–59683
47. Wang Y, Yang F, Yang X (2010) Label-free colorimetric biosensing of copper (II) ions with unimolecular self-cleaving deoxyribozymes and unmodified gold nanoparticle probes. Nanotechnology 21(20):205502